Rapid Communications

Time-of-flight electron scattering from molecular hydrogen: Benchmark cross sections for excitation of the $X\,^1\Sigma_g^+ \rightarrow b\,^3\Sigma_u^+$ transition

M. Zawadzki,[1] R. Wright,[2] G. Dolmat,[2] M. F. Martin,[2] L. Hargreaves,[2] D. V. Fursa,[3] M. C. Zammit,[4] L. H. Scarlett,[3] J. K. Tapley,[3] J. S. Savage,[3] I. Bray,[3] and M. A. Khakoo[2,*]

[1]*Atomic Physics Division, Department of Atomic, Molecular, and Optical Physics, Faculty of Applied Physics and Mathematics, Gdańsk University of Technology, ul. G. Narutowicza 11/12, 80-233 Gdańsk, Poland*

[2]*Department of Physics, California State University, Fullerton, California 92831, USA*

[3]*Curtin Institute for Computation and Department of Physics, Astronomy and Medical Radiation Sciences, Curtin University, Perth, Western Australia 6102, Australia*

[4]*Theoretical Division, Los Alamos National Laboratory, Los Alamos, New Mexico 87545, USA*

(Received 8 March 2018; published 24 May 2018)

The electron impact $X\,^1\Sigma_g^+ \rightarrow b\,^3\Sigma_u^+$ transition in molecular hydrogen is one of the most important dissociation pathways to forming atomic hydrogen atoms, and is of great importance in modeling astrophysical and industrial plasmas where molecular hydrogen is a substantial constituent. Recently, it has been found that the convergent close-coupling (CCC) cross sections of Zammit *et al.* [Phys. Rev. A **95**, 022708 (2017)] are up to a factor of 2 smaller than the currently recommended data. We have determined normalized differential cross sections for excitation of this transition from our experimental ratios of the inelastic to elastic scattering of electrons by molecular hydrogen using a transmission-free time-of-flight electron spectrometer, and find excellent agreement with the CCC calculations. Since there is already excellent agreement for the absolute elastic differential cross sections, we establish benchmark differential and integrated cross sections for the $X\,^1\Sigma_g^+ \rightarrow b\,^3\Sigma_u^+$ transition, with theory and experiment being essentially in complete agreement.

DOI: 10.1103/PhysRevA.97.050702

The hydrogen molecule H_2 is the simplest neutral molecule, the most abundant molecule in the universe, and is the main constituent in the atmospheres of the outer planets. The electron impact excitation of the $X\,^1\Sigma_g^+ \rightarrow b\,^3\Sigma_u^+$ transition in molecular hydrogen is as fundamental a process as the comparable atomic excitation of the $1S \rightarrow 2S, 2P$ levels of hydrogen. Excitation of H_2 into the repulsive $b\,^3\Sigma_u^+$ state is a major process by which H_2 is dissociated into neutral H($1S$) atoms. Accurate data for molecular hydrogen dissociation is of crucial importance for many applications ranging from astrophysics and fusion research [1] to material science and combustion physics [2]. For example, the modeling of stellar formation mechanisms [3] and strong H_2 emission [4] of primordial gas clouds relies on the understanding of the nonequilibrium H_2 chemistry (production, destruction, cooling, and heating) of primordial gas clouds exposed to external ionizing radiation sources, where suprathermal secondary electrons are produced typically with energy in the range of 20–40 eV [4,5].

In 1990, recognizing the importance of e^--H_2 processes, Tawara *et al.* [6] published a comprehensive compilation of cross-section data regarding electron collisions with H_2. In 2008 this list was updated by Yoon *et al.* [7] and a set of recommended cross sections was specified. The latter were predominantly compiled from available experimental data that were often few and in some cases had large uncertainties.

The dissociation of H_2 by electron impact was, amazingly, inferred only from a famous experiment of Corrigan in 1965 [8] where the dissociated H atoms were trapped by adsorption into molybdenum trioxide, in a low out-gassing vacuum chamber. This experiment provided a remarkably good estimate for dissociation via all reaction channels. The dissociation via the repulsive $b\,^3\Sigma_u^+$ state was investigated in several experiments where the differential cross section (DCS) for excitation of the $X\,^1\Sigma_g^+ \rightarrow b\,^3\Sigma_u^+$ transition in H_2 were measured by Hall and Andric [9], Nishimura and Danjo [10], Khakoo *et al.* [11], and Khakoo and Segura [12], using electrostatic electron energy-loss spectrometry. These data range from incident electron energies (E_0) of 9–60 eV, for scattering angles (θ) from 10° to 130°.

A theoretical treatment of electron impact excitation of the $b\,^3\Sigma_u^+$ state of H_2 exhibits difficulties characteristic to electron-molecule collisions in general. At energies close to the excitation threshold the effects of nuclear motion have to be taken into account, and as incident electron energy increases, interchannel coupling plays a dominant role, both making theoretical treatments extremely difficult. While a large number of theoretical methods have been applied to calculation of the $b\,^3\Sigma_u^+$ excitation, they are in significant disagreement with each other and with the recommended data (refer to Scarlett *et al.* [13] for references and more detailed discussion). A recent breakthrough in the theoretical adaptation of the convergent close-coupling (CCC) model of Bray and co-workers [14,15], which had been very successful for electron scattering from two-electron atoms, was applied to electron scattering from molecular hydrogen. Comparison of the electron impact excitation of the H_2 DCS from the molecular CCC of Zammit *et al.* [16] with experimental data

*Corresponding author: mkhakoo@fullerton.edu

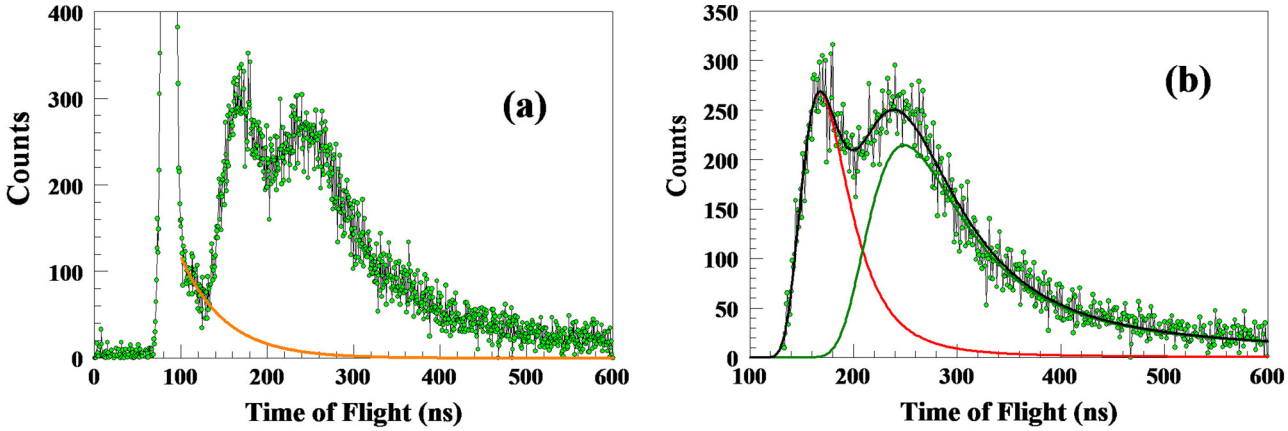

FIG. 1. (a) Background subtracted time-of-flight spectrum for electron scattering from H_2 taken at $E_0 = 15$ eV and $\theta = 90^\circ$ showing the exponential tail of the elastic peak (orange line). (b) Inelastic part of (a) with exponential tail of elastic peak subtracted. The spectrum is fitted to the Franck-Condon envelope (red line) for the $X\,^1\Sigma_g^+ \rightarrow b\,^3\Sigma_u^+$ transition [27] and a function (green line) which represents the bound higher states of H_2 to fit the remaining spectrum [Eq. (1)], above the $b\,^3\Sigma_u^+$. Time is referenced relative to the crossing of electron pulse over the collision region. See text for discussion.

from the California State University Fullerton (CSUF) group for excitation of the $X\,^1\Sigma_g{}^+ \rightarrow a^3\Sigma_g{}^+$, $c^3\Pi_u$, $B^1\Sigma_u{}^+$, $C^1\Pi_u$, and $E,F\,^1\Sigma_g{}^+$ transitions showed good agreement in many cases—certainly much improved over the existing theories. The account of nuclear motion becomes progressively more important as the incident electron energy becomes smaller. The adiabatic nuclei CCC approach [13] proved to be in good agreement with the experiment for energies below 13 eV. However, the agreement of the excitation DCS for the $X\,^1\Sigma_g^+ \rightarrow b\,^3\Sigma_u^+$ transition in H_2 with theory was poor at incident energies above 13 eV with the largest, nearly a factor of 2, discrepancies in some cases. Moreover, the experimental integrated cross sections (ICS) predicted the cross-section maximum at 15 eV (see, e.g., [7]) while the CCC results have the considerably smaller maximum at 12 eV. This large disagreement for such a fundamental cross section is certainly extremely worrisome and requires careful analysis of both theoretical and experimental techniques.

The CCC method [16], for molecules, utilizes large close-coupling expansions to describe e^--H_2 collisions. The set of H_2 target states used in such expansions is obtained via diagonalization of the H_2 Hamiltonian in a Sturmian (Laguerre) basis that allows it to model all important reaction channels including ionization. Zammit *et al.* [16] has used the fixed-nuclei formulation of the CCC method and demonstrated the convergence of the calculated cross sections with respect to the increasing size of the close-coupling expansion. Scarlett *et al.* [13] has applied the adiabatic nuclei formulation of the CCC method to the $X\,^1\Sigma_g^+ \rightarrow b\,^3\Sigma_u^+$ excitation. They demonstrated that nuclear motion effects become negligible above 13–14 eV E_0 values. Considerable effort has been directed to establish numerical stability of the obtained cross sections and provide the combined uncertainty of the theoretical results that was estimated to be better than 10%. Given the detailed analysis conducted to test the theoretical results, it was concluded that the discrepancy between theory and experiment is unlikely to be due to the deficiencies in the theoretical treatment of the problem. A possibility for the experiment to overestimate the cross section for the $b\,^3\Sigma_u^+$ state excitation could, in principle, be due to the cascading from higher lying triplet states. In fact, Scarlett *et al.* [17] has shown that the cascading contribution has a maximum at 16 eV and becomes larger than the direct $b\,^3\Sigma_u^+$ excitation cross section above 14 eV. However, the DCS measurements [9–12] are free from cascading and therefore, cannot explain the factor of 2 discrepancies, in some cases, between theory and experiment.

On the experimental side there is a possible error in calibrating out the transmission of conventional electron-scattering spectrometers. In principle, the $X\,^1\Sigma_g^+ \rightarrow b\,^3\Sigma_u^+$ transition is 68% exposed in the energy-loss spectrum, with the rest overlapping with the higher lying excited bound states of H_2, which themselves are heavily overlapped and have to be unfolded to extract individual state excitation DCSs [18]. Since it is the most exposed, it should be possible to determine its excitation DCS more accurately than those of the heavily overlapped higher lying states.

To get reliable *quantitative* experimental DCSs at least in the 20% error range or better, we decided to build a differential scattering electron time-of-flight (TOF) spectrometer because such devices, in principle, should not suffer from transmission problems (as long as the remnant magnetic field in the experiment is below 2 mG). This was well demonstrated by Le Clair *et al.* [19] who built a fixed 90°, scattering angle (θ) device as a first operating TOF spectrometer, operating at a repetition rate of 100 kHz with the pulsed electrons produced by sweeping the unselected electron beam (0.5 eV resolution) across an aperture. Clair *et al.* measured inelastic to elastic ratios for H, Xe, CO, and N_2, but at a fixed θ of 90°. A more sophisticated system capable of θ from 45° to 130°, with a higher energy resolution (60–80 meV) pulsed beam was built by the Australian National University group [20] and was used to measure the excitation of He $n = 2,3$ levels at $E_0 = 20.35$, 22.0, and 23.48 eV [21]. Similarly as in [19] the beam was pulsed by sweeping it across an aperture at a repetition rate of 500 kHz.

At CSUF we have developed a TOF system that is significantly different from the previous in that

(i) the electron beam is pulsed by pulsing a thin aperture lens in between the filament and anode using a 0–40 V, 0.5–10 ns

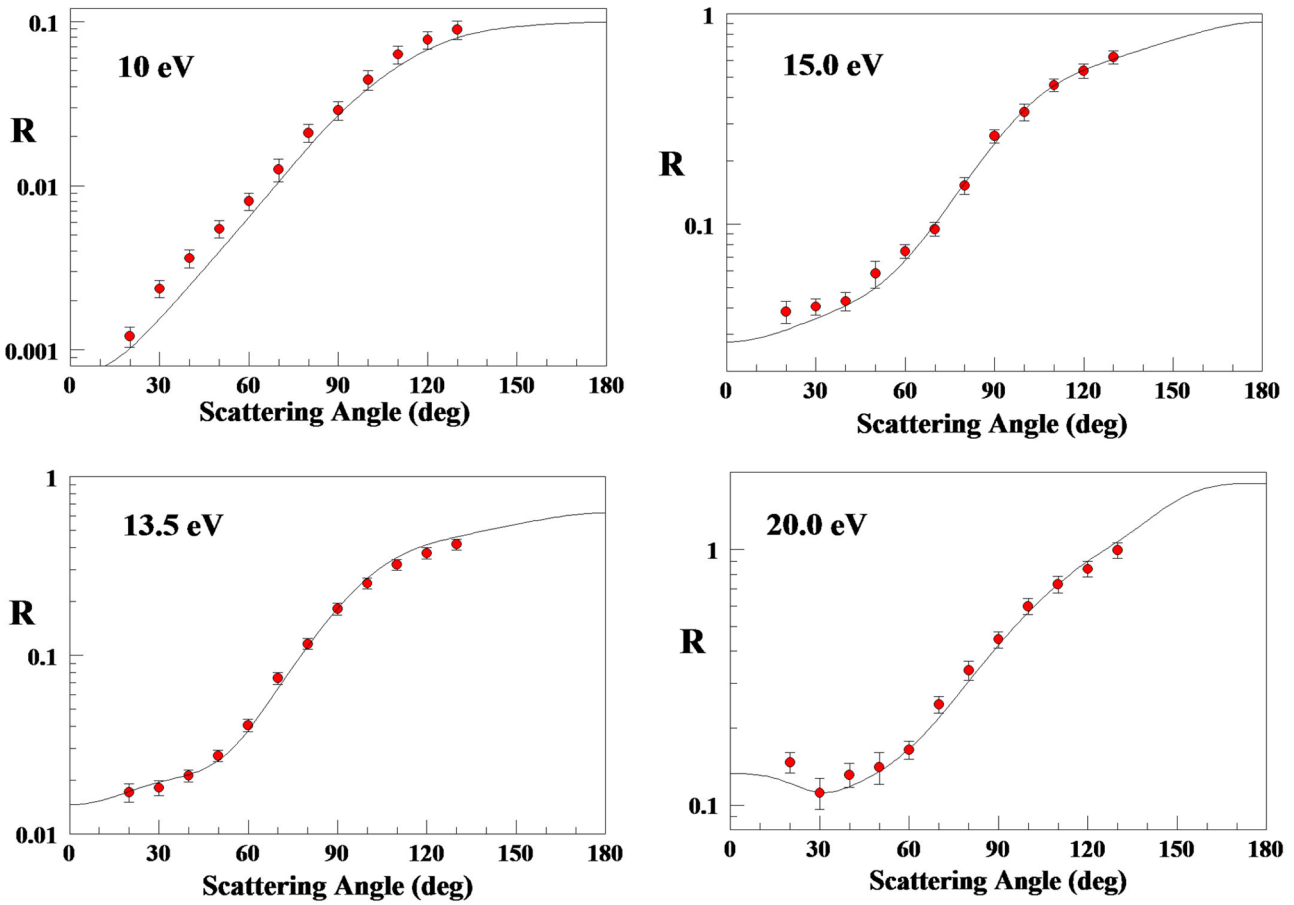

FIG. 2. Inelastic to elastic ratios R at various E_0 values. Legend: ●, present results from TOF experiment with one standard deviation error bars; ——, present CCC.

pulse generator [22] wired in an impedance matched coaxial cable circuit;

(ii) the TOF tube was made compact, but long (23.9 cm TOF distance, 3.3 cm outer diameter) and able to rotate up until $\theta = 135°$. It had an aluminum body which was coated with sprayed colloidal graphite, but had a tapered nose piece made of titanium, which had an opening of 2 mm diameter. The opening aperture area was not coated with graphite. The TOF tube had four tandem thin molybdenum apertures (0.07 mm thick), placed to subtend the same solid angle to the center of the collision region in an effort to reject secondary electrons. This system was heated by electrically shielded, biaxial, magnetically free heaters [23] to a temperature of 90–150 °C;

(iii) it had an open grounded collision region, without biased grids [20] or electron traps [19] in front of or opposite to the TOF tube, but used an acetylene flame sooted molybdenum hypodermic needle incorporated into a movable source system developed at CSUF [24] which expediently enabled the determination of backgrounds in the scattering experiment; and

(iv) the detector is a multichannel plate similar to the other systems (ours is a triple microchannel plate system, 1 in. in diameter [25]), whose front was biased at +300 V with respect to ground to attract electrons; this potential was isolated somewhat differently from the grounded TOF tube using a single 95% transparency 2.5 mm square, grounded tungsten grid which was sprayed lightly with colloidal graphite, which was found to work adequately after many tests with other grid-type and slat-type setups (see, e.g., [19,20]).

The system was placed in a mu-metal lined chamber with a single vertical Helmholtz coil which was able to reduce the remnant B field of the Earth in the laboratory to less than ±2 mG over a radius of 30 cm around the collision region and it was only when this B field was reduced that the instrument began to work well. The electron beam was pulsed by a capacitive coupled positive going pulse, 2–2.5 ns and 5–8 V in amplitude, with the pulsed aperture biased at a negative potential of −5 to −8 V to cut out a DC flow of electrons. It produced 1–5 μA peak current pulsed beams at the 500 kHz repetition rate with widths of ≈3 ns. The energy of the beam was determined accurately within ±0.15 eV using the TOF times of the $b\,^3\Sigma_u^+$ feature at 10.19 eV energy loss and the $C\,^1\Pi_u$ peak at 12.57 eV energy loss as well as the delay from prompt UV photons and the elastic peak. The gun had two small ≈1 mm apertures to collimate the beam, with an angular spread of about 3°. The sooted molybdenum movable target needle was placed 6 mm below the center of the collision region to provide negligible electron scattering from it. The clean vacuum system was pumped by three, 6-in. oil-free turbomolecular pumps, with a base pressure of around 1×10^{-7} torr or better with bakeouts fully on. The system was always vented to dry nitrogen, and was allowed to cool after

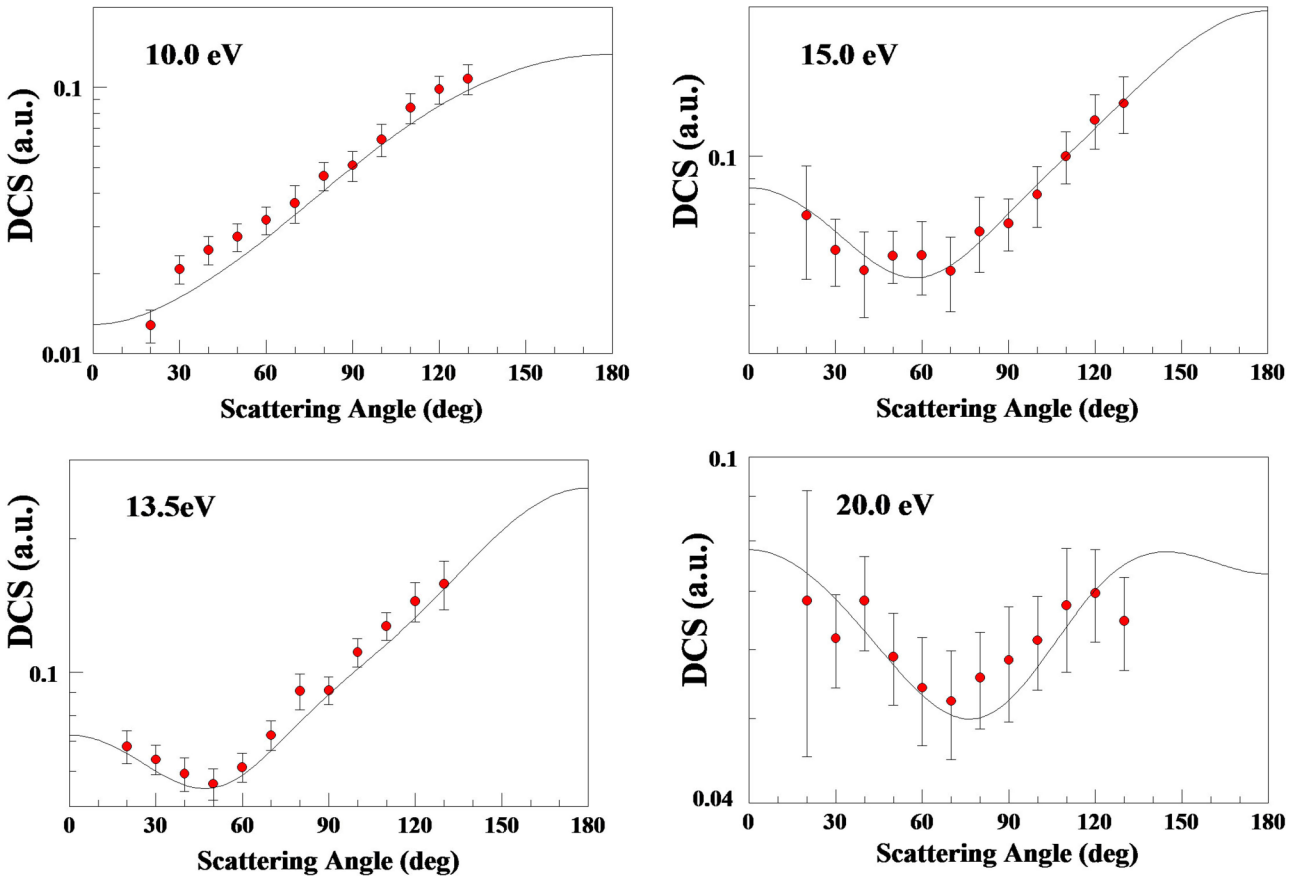

FIG. 3. DCS in atomic units for excitation of the $b\,^3\Sigma_u^+$ state at various E_0 values. Legend is the same as for Fig. 2.

which the vacuum chamber was opened for servicing to ensure cleanliness. Full details of this instrument will be published in a methods paper to come.

Typical electron-scattering signal rates were around 200 to >5000 Hz. Figure 1 shows a TOF spectrum for H_2 at $E_0 = 15$ eV taken at $\theta = 90°$. The spectrum is obtained by subtracting the background scattering with the gas beam collimator displaced away from the collision region from the signal plus background scattering with the gas beam collimator in place in the collision region [24]. From such spectra we can determine accurate inelastic to elastic ratios (R) after removing an exponential contribution from the elastic peak's tail, which is produced by collisions of electrons with the gas and surfaces in the TOF tube [20]. Typical signal+background to background ratios were between 3:1 and 2:1. We note that since the slower electrons are easier to deflect from the line of sight with the electron detector (by B fields and by dirt on the TOF tube optics), in principle one would expect that the higher R the better the measurement. At energies above the H_2 ionization potential of 15.43 eV [26], however, both target-ionized ejected electrons are detected as well as those projectile scattered after ionizing the target. In this case it is necessary to separate inelastic electrons scattered from exciting bound states of H_2 and of the ionization continuum above 15.43 eV energy loss. Thus the ratios R presented are those which compare inelastic electrons scattered from exciting bound states and the vibrationally elastic scattered electrons. We have taken TOF spectra at E_0 values of 10, 11, 12.5, 13, 13.5, 14, 15, 15.5, 16, 17.5, 20, and 25 eV for θ of 20°–130°.

The elastic peak intensity was determined by integrating the counts under this feature. For certain energies the exponentially decaying elastic tail overlapped with the $b\,^3\Sigma_u^+$ peak. Hence, prior to applying the fitting procedure to the $X\,^1\Sigma_g^+ \rightarrow b\,^3\Sigma_u^+$ feature we fitted and subtracted the exponential tail from the elastic peak. To determine the DCS of the excitation of the $X\,^1\Sigma_g^+ \rightarrow b\,^3\Sigma_u^+$ transition, the TOF spectra were fitted to the Franck-Condon envelope of the $X^1\Sigma_g{}^+(v'' = 0) \rightarrow b\,^3\Sigma_u^+$ repulsive potential from Rescigno *et al.* [27] weighted by the flux factor k_f/k_i where k_f is the scattered electron momentum and k_i is the incident electron momentum (see also [11,12]), in the TOF coordinates and not converting into energy-loss space. The remaining inelastic spectrum, excluding ionization, was approximated using a similar function for the $X\,^1\Sigma_g^+ \rightarrow b\,^3\Sigma_u^+$ feature:

$$f(t) = A\exp[-(\alpha/t^2 - \mu)/\sigma], \tag{1}$$

where the TOF is given by t, the intensity given by A, the scale time factor α (which is a numerical constant dependent on the timescale), the mean position is μ, and the width σ were nonlinearly fitted to the rest of the inelastic features. The sum of two fitting functions, for the $X\,^1\Sigma_g^+ \rightarrow b\,^3\Sigma_u^+$ state and the higher bound states of H_2, reproduced the inelastic transition features very well. DCSs for the inelastic features were determined by normalizing the intensity of the elastic-scattering peak to our experimental DCSs of Muse *et al.* [28] and scaling up the inelastic components correspondingly.

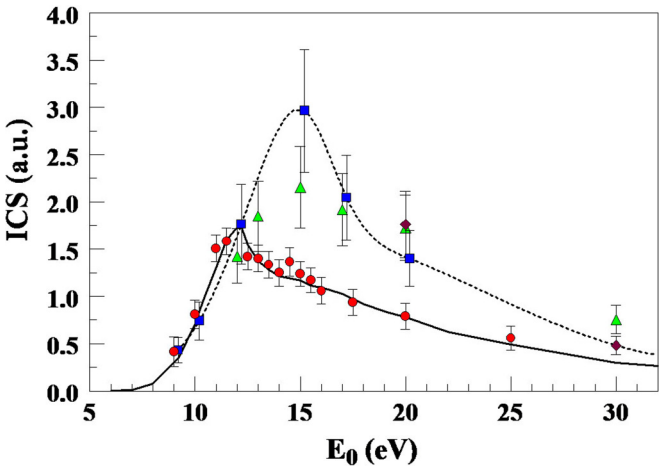

FIG. 4. ICSs in atomic units for excitation of the $b\,^3\Sigma_u^+$ state at various E_0 values. Legend is the same as for Fig. 2 except ▲, Nishimura and Danjo [10]; ◆, Khakoo *et al.* [11]; ■, Khakoo and Segura [12]. Note, the recommended ICSs by Yoon *et al.* [7]: ----- are the ICSs of [12] from 9.2V to 20 eV and ICSs of [11] from 30 to 100 eV.

Figure 2 shows typical R values from this experiment compared with the CCC. The measurements at 10 eV are slightly larger than theory by about 20% at small θ, but in very good agreement within the experimental error bars at higher θ. At the higher energies agreement is excellent and well within error bars of about 12%–15%. We note somewhat raised deviation between theory and experiment at the forward-scattering angles due to raised background from the forward electron beam, which is mostly, but probably not completely, removed by using the movable target source arrangement. Previously, when the remnant B fields were in the region of ≈40 mG, the ratios were in worse agreement with theory, in cases around low E_0 by factors of up to 2.

In Fig. 3 we present the $b\,^3\Sigma_u^+$ DCSs, and note the excellent agreement of experiment with theory, which is presently unprecedented for electron-molecule excitation processes. Although not presented here, the CCC-calculated elastic DCSs are in excellent agreement with experiment [28]; see also reference [18] for comparisons at $E_0 = 15$ and 17.5 eV. A comprehensive presentation of these DCSs over a broad energy range from low to high energies will be presented elsewhere.

Figure 4 shows the ICSs for excitation of the $X\,^1\Sigma_g^+ \rightarrow b\,^3\Sigma_u^+$ transition. The excitation function shows a much different shape than previous ICS determinations by [10] and [12]. Both show reasonable values except at 15 eV where [12] is much higher than present values by a factor of almost 2 with an error of around ±30%. The previously recommended ICSs [7] are also substantially higher than the currently measured ICS and the CCC theory, which are in excellent agreement with each other.

Interestingly, the $b\,^3\Sigma_u^+$ state excitation ICS falls sharply after the maximum at 12 eV, which is most likely due to interchannel coupling of the extended $b\,^3\Sigma_u^+$ state (continuum) with the near-degenerate bound triplet states in this energy region, e.g., the $a^3\Sigma_g{}^+$ and $c^3\Pi_u$ states. Hence, the spin-exchange process that excites the $b\,^3\Sigma_u^+$ state will also couple the other excitations for these triplets, since spin-orbit coupling with the projectile electron is expected to be small for a light target as H_2. We have not experimentally investigated the role of resonances in the region of $E_0 = 11.75$–12.25 eV which affect the rapid changes in the angular distribution of the $b\,^3\Sigma_u^+$ state DCSs (as observed by the present CCC), but will do this as a separate project following this work.

In conclusion, we have used a recently built TOF system that is not susceptible to transmission effects and can accurately give inelastic to elastic ratios for (in this case) electron excitation of H_2. The absolute DCS for excitation of the $b\,^3\Sigma_u^+$ state of H_2 was determined after normalizing the unfolded TOF spectrum to the experimental elastic DCS of Muse *et al.* [28]. Excellent agreement of experiment with the CCC calculations is found for both the total inelastic to elastic ratio and the absolute DCS. This resolves the previously existing discrepancies between experiment and theory for this fundamentally important excitation process. It is hoped that this collaboration between theory and experiment will make significant contributions to determine accurate cross sections for excitation of other atomic and molecular targets.

M.Z. acknowledges support from the Fulbright Fellowship program. This experimental work was supported by the US National Science Foundation Research in an Undergraduate Institution under Grant No. NSF-RUI-PHY-1606905 to M.A.K. This theoretical work was supported by the United States Air Force Office of Scientific Research, Los Alamos National Laboratory (LANL) and Curtin University. M.C.Z. would like to specifically acknowledge LANs ASC PEM Atomic Physics Project for its support. LANL is operated by Los Alamos National Security, LLC for the National Nuclear Security Administration of the US Department of Energy under Contract No. DE-AC52-06NA25396. L.H.S. acknowledges the contribution of an Australian Government Research Training Program Scholarship, and the support of the Forrest Research Foundation. Resources were provided by the Pawsey Supercomputing Centre with funding from the Australian government and the government of Western Australia.

[1] J. P. Boeuf, G. J. M. Hagelaar, P. Sarrailh, G. Fubiani, and N. Kohen, Plasma Sources Sci. Technol. **20**, 015002 (2011).
[2] Y. Ju and W. Sun, Prog. Energy Combust. Sci. **48**, 21 (2015).
[3] N. Yoshida, Astrophys. J. **663**, 687 (2007).
[4] G. J. Ferland, A. C. Fabian, N. A. Hatch, R. M. Johnstone, R. L. Porter, P. A. M. van Hoof, and R. J. R. Williams, Mon. Not. R. Astron. Soc. **392**, 1475 (2009).

[5] M. L. Lykins, G. J. Ferland, R. Kisielius, M. Chatzikos, R. L. Porter, P. A. M. van Hoof, R. J. R. Williams, F. P. Keenan, and P. C. Stancil, Astrophys. J. **807**, 118 (2015).
[6] H. Tawara, Y. Itikawa, H. Nishimura, and M. Yoshino, J. Phys. Chem. Ref. Data **19**, 617 (1990).
[7] J.-S. Yoon, M.-Y. Song, J.-M. Han, S. H. Hwang, W.-S. Chang, B. J. Lee, and Y. Itikawa, J. Phys. Chem. Ref. Data **37**, 913 (2008).
[8] S. J. B. Corrigan, J. Chem. Phys. **43**, 4381 (1965).
[9] R. I. Hall and L. Andric, J. Phys. B: At. Mol. Phys. **17**, 3815 (1984).
[10] H. Nishimura and A. Danjo, J. Phys. Soc. Jpn. **55**, 3031 (1986).
[11] M. A. Khakoo, S. Trajmar, R. McAdams, and T. Shyn, Phys. Rev. A **35**, 2832 (1987).
[12] M. A. Khakoo and J. Segura, J. Phys. B: At. Mol. Phys. **27**, 2355 (1994).
[13] L. H. Scarlett, J. K. Tapley, D. V. Fursa, M. C. Zammit, J. S. Savage, and I. Bray, Phys. Rev. A **96**, 062708 (2017).
[14] I. Bray and A. T. Stelbovics, Phys. Rev. A **46**, 6995 (1992).
[15] D. V. Fursa and I. Bray, Phys. Rev. A **52**, 1279 (1995).
[16] M. Zammit, J. S. Savage, D. V. Fursa and I. Bray, Phys. Rev. A **95**, 022708 (2017).
[17] L. H. Scarlett, J. K. Tapley, D. V. Fursa, M. C. Zammit, J. S. Savage, and I. Bray, Eur. J. Phys. D **72**, 34 (2018).
[18] L. R. Hargreaves, S. Bhari, B. Adjari, X. Liu, R. Laher, M. Zammit, J. S. Savage, D. V. Fursa, I. Bray, and M. A. Khakoo, J. Phys. B: At., Mol. Opt. Phys. **50**, 225203 (2017).
[19] L. R. LeClair, S. Trajmar, M. A. Khakoo, and J. C. Nickel, Rev. Sci. Instrum. **67**, 1753 (1996).
[20] M. Lange, J. Matsumoto, A. Setiawan, R. Panajotović, J. Harrison, J. C. A. Lower, D. S. Newman, S. Mondal, and S. J. Buckman, Rev. Sci. Instrum. **79**, 043105 (2008).
[21] M. Lange, J. Matsumoto, J. Lower, S. Buckman, O. Zatsarinny, K. Bartschat, I. Bray, and D. Fursa, J. Phys. B: At., Mol. Opt. Phys. **39**, 4179 (2006).
[22] Model AVR-E5-B-05, Avtech Electrosystems Ltd., Ogdensburg, NY.
[23] 1HN040B-16.3 biaxial cable, ARi Industries Inc., Addison, IL.
[24] M. Hughes, K. E. James, Jr., J. G. Childers, and M. A. Khakoo, Meas. Sci. Technol. **14**, 841 (1994).
[25] Z-stack, APD 3 MA 25/12/10/12 D 60:1, PHOTONIS USA, Inc., Sturbridge, MA.
[26] J. Liu, E. J. Salumbides, U. Hollenstein, J. C. J. Koelemeij, K. S. E. Eikema, W. Ubachs, and Frédéric Merkt, J. Chem. Phys. **130**, 174306 (2009).
[27] T. N. Rescigno, C. W. McCurdy, Jr., V. McKoy, and C. F. Bender, Phys. Rev. A **13**, 216 (1976).
[28] J. Muse, H. Silva, M. C. A. Lopes, and M. A. Khakoo, J. Phys. B: At., Mol. Opt. Phys. **41**, 095203 (2008).